Catal Lett (2009) 127:448–455
DOI 10.1007/s10562-008-9739-3

Effect of Lanthanum Promotion on the Unsupported Mo–Co–K Sulfide Catalysts for Synthesis of Mixed Alcohols from Syngas

Yong Yang · Yangdong Wang · Su Liu · Qingying Song · Zaiku Xie · Zi Gao

Received: 20 August 2008 / Accepted: 16 October 2008 / Published online: 13 November 2008

Abstract The unsupported Mo–Co–K sulfide catalysts promoted by La were prepared through ultrasonic technology in non-aqueous medium and its performances for the synthesis of mixed alcohols from syngas were also investigated. The results showed that the catalysts promoted by La exhibited higher CO conversion and selectivity to ethanol than the unsupported Mo–Co–K sulfide catalyst without addition of La did under identical reaction conditions. The catalysts were characterized by N_2 adsorption/desorption, X-ray diffraction (XRD), Scanning electron microscope (SEM), Transmission electron microscope (TEM), Raman, and X-ray photoelectron spectroscopy (XPS).

Keywords Syngas · Ethanol · Mixed alcohols · Rare earth · Unsupported Mo–Co–K sulfide catalyst

1 Introduction

Much attention has been paid to mixed alcohols synthesis due to its properties as the gasoline blend or alternative motor fuel for the reduction of exhaust emission in the last 20 years. The addition of oxygenates, such as alcohols and ethers, into gasoline give rise to decreased toxic exhaust gas (CO, NO_x) and in some cases increase octane number. Especially, use of methyl *tert*-butyl ether (MTBE) has been prohibited recently in some countries or regions as additive of oil-based fuel due to the new legal requirements in environment protection. So, as a potential alternative fuel or additive, the catalytic conversion of synthesis gas to mixed alcohols is now attracting renewed attention for both industrial application and fundamental research.

Attempts have been taken to develop new catalysts to improve the catalytic activity and selectivity to mixed alcohols. Recent studies revealed that both the activity and selectivity to higher alcohols can be improved by adding effective promoters, such as Fischer-Tropsch components and alkali metals into MoS_2-based catalysts [1–5], changing the nature of the catalyst supports [6–11], and modifying the catalyst preparation method [12, 13]. Very recently, other new catalysts were also developed and a good activity and selectivity could also be obtained. For instance, Kaliaguine et al. [14, 15] reported conversion of syngas to higher alcohols over nanocrystalline Co–Cu-based perovskites as catalysts, and Xiang et al. [16, 17] reported synthesis of higher alcohols from syngas over Fischer-Tropsch elements modified molybdenum carbides. However, up to now, from the viewpoint of practical use, among various catalysts, alkali-doped MoS_2 catalysts are still considered the most promising due to their resistance to sulfur poisoning and high activity for the water-gas shift reaction.

To design unsupported MoS_2 based catalysts, it is essential to properly introduce the modifier and preparation method to improve its catalytic activity. The 3d transition metals such as Co, Fe, Ni, Rh, et al. were introduced into alkali-doped MoS_2 catalysts system [18–21]. Generally, it was considered that at least two forms of transition metal promoters simultaneously existed in MoS_2 based catalysts, namely, separated phases of transition metal sulfides and mixed phases such as so-called "Mo–M–S"

Y. Yang (✉) · Y. Wang · S. Liu · Q. Song · Z. Xie
Shanghai Research Institute of Petrochemical Technology, Shanghai 201208, People's Republic of China
e-mail: yongyang24@yahoo.com.cn

Y. Yang · Z. Gao
Department of Chemistry, Fudan University, Shanghai 200433, People's Republic of China

(M = transition metals) [22, 23]. And it has been recognized that the close interaction between Mo and promoter atoms also exerted great influence on promotion effects for mixed alcohols synthesis from syngas. Moreover, the structural and morphology of metal promoter and MoS_2 support was closely related to the promotion effects. As a potential element, it has been reported that the addition of La or Ce into supported Ni and supported Co catalysts gave increased catalytic activity [24–26]. The results demonstrated that the roles of the rare earths are as structural promoters, chemical promoters, or synergetic promoters. Ogawa et al. [27] introduced La into Ni–Mo/alumina supported catalysts and investigated its effects on the structural and catalytic activity for hydrodesulfurization (HDS). They found that La loading significantly affected the surface concentration of active components and the structural of MoS_2 crystallites, which resulted in the increase of the HDS reaction. However, few works of the La promoted unsupported MoS_2 based catalysts have been reported systematically for the synthesis of mixed alcohols from syngas.

The aim of the present work is to explore the effect of the La on between the catalyst structure and its catalytic performance after addition into the unsupported Mo–Co–K sulfide catalysts for the synthesis of mixed alcohols from syngas through careful characterization of XRD, N_2 adsorption/desorption, Scanning electron microscope (SEM), HRTEM, Raman and X-ray photoelectron spectroscopy (XPS).

2 Experimental

2.1 Catalyst Preparation

The catalysts were prepared by an ultrasonic technology in a non-aqueous medium. As a typical synthesis, tow non-aqueous solutions were prepared (A and B). Solution A consisted of $Co(CH_3COO)_2$ and rare earth metal nitrate dissolved in ethanol, solution B consisted of $(NH_4)_2MoS_4$ dissolved in ethanol. After the solution A was treated 30 min at room temperature under high-ultrasound environmental, solution B was dropped into the mixture and followed by treatment with ultrasonic apparatus till the black precipitates were formed. The precipitate was aged at room temperature overnight, and then filtered. The filtered cake (precipitate) was repeatedly rinsed with ethanol. The obtained solid was dried at 120 °C for 12 h, followed by mixing with K_2CO_3 to thermal decomposition at 500 °C under N_2 for 2 h to obtain La-promoted unsupported Mo–Co–K sulfidecatalyst. The Mo–Co–K sulfide catalysts promoted by rare earth (La, Ce, or Y) are denoted as $M_xMoCo_yK_z$, where M is the rare earth, x, y, and z are the molar ratio of M/Mo, Co/Mo, K/Mo, respectively.

2.2 Catalyst Test

The catalytic test was carried out in a fixed-bed reactor with equipped with on-line gas chromatograph. For each experiment, 0.8 mL sample was charged into a stainless-steel reactor with I. D. of 6 mm. The synthesis gas was composed of CO (30%), H_2 (60%) and N_2 (10%). Reaction conditions were: temperature = 330 °C, pressure = 3.0 MPa, and GHSV = 2,225 h^{-1}. The products were analyzed by gas chromatographs (HP-4890) after the reaction for 24 h when a steady state activity appeared. H_2, CO, CH_4, and CO_2 were monitored by TCD using H_2 as the carrier gas. The capillary column (Propake-Q) was connected to an FID using nitrogen as the carrier gas to separate all of the C1–C5 alcohols and the C1–C6 hydrocarbons. CO conversion and CO_2 selectivity were determined using an internal standard, and the carbon-based selectivity of the carbon-containing products (including alcohols, alkanes, and other oxygenates) was calculated by an internal normalization method.

2.3 Characterization

The catalysts were characterized by XRD, N_2 adsorption/desorption, SEM, Transmission electron microscope (TEM), Raman and XPS. The powder XRD patterns were recorded at room temperature on a Bruker-AXS D8 Advance X-ray diffractometer using Cu–Ka radiation in 40 kV and 200 mA. The θ angles were scanned from 5 to 70° at a rate of 5°/min. Brunauer–Emmett–Teller (BET) surface areas of the catalysts were determined from N_2 adsorption/desorption measurements at 77 K with a Micromeritics Tristar 3000 (Carlo Erba) system. The sample was outgassed under vacuum at 250 °C for 3 h before the adsorption of nitrogen. SEM images were taken with a XL30E electron probe X-ray microanalyzer. Chemical compositions were examined by EDS using XL30E electron microscope. For the SEM observations, the samples were deposited on a sample holder and coated with Au. High-resolution TEM (HRTEM) images were obtained on a Philips TECNAI F-30 FEG instrument at an accelerating voltage of 300 kV. The sample was dispersed with dry ethanol. Raman spectroscopy was recorded with LabRam 1B spectrometer. The excitation power of the 632.8 nm line of the YAG laser was fixed at 4.3 mW. XPS measurements were recorded on a Quantum 2000 Scanning ESCA Microprobe instrument with Al Ka radiation (15 kV, 25 W, hv = 1486.6 eV). The pressure in the sample chamber was around 4×10^{-7} Pa. The sample

temperature was 20 °C. All the binding energies (BE) were referenced to the C1 s oine at 284.6 eV.

3 Results and Discussion

3.1 Metal Composition on the Surface and Surface Area of Catalysts

Table 1 lists the results of metal composition on catalysts surface measured by EDS and surface area of the as-prepared catalysts. As shown in Table 1, the surface S/Mo ratios of catalyst $La_xMoCo_{0.5}K_{0.6}$ ($x = 0.1$, 0.2, 0.3) are very close to the stoichiometric MoS_2 compositions, and the surface Co/Mo, K/Mo, and La/Mo ratios are also very close to that in the bulk of catalysts. However, the surface S/Mo ratio in $MoCo_{0.5}K_{0.6}$ catalyst is somewhat higher than the stoichiometric MoS_2 compositions; and especially, the surface Co/Mo ratio is far bigger than that in the bulk of catalyst (Co/Mo = 0.5), which might be due to the possibility that the separated aggregates of CoS_x particles were gathered on the surface of the catalyst $MoCo_{0.5}K_{0.6}$.

All the catalysts exhibited relatively low BET surface area values of 3–10 m^2/g. The surface area of the as-prepared catalysts was slightly lower than that of the pure MoS_2 crystallites, and it increased with increasing La/Mo molar ratio, whereas the surface area decreased with further increasing La/Mo molar ration (above 0.2).

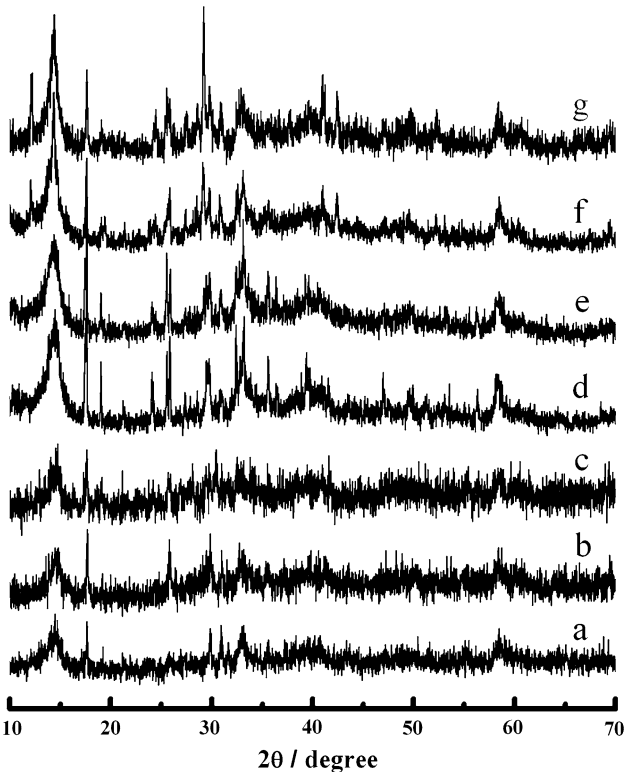

Fig. 1 The XRD patterns for the Mo–Co–K sulfide catalysts with or without the addition of rare earths. (a) $MoCo_{0.5}K_{0.6}$; (b) $Ce_{0.2}MoCo_{0.5}K_{0.6}$; (c) $Y_{0.2}MoCo_{0.5}K_{0.6}$; (d) $La_{0.1}MoCo_{0.5}K_{0.6}$; (e) $La_{0.2}MoCo_{0.5}K_{0.6}$; (f) $La_{0.3}MoCo_{0.5}K_{0.6}$; (g) $La_{0.6}MoCo_{0.5}K_{0.6}$

3.2 Characterization of X-ray Diffraction (XRD)

Figure 1 shows the XRD patterns for the unsupported Mo–Co–K sulfide catalysts before and after addition of rare earths. In all cases, the diffraction indicated the poorly crystalline hexagonal MoS_2 with the broad reflection peaks at 2θ (degree) = 14.4, 33.3, 39.7 and 58.7, respectively. For the $MoCo_{0.5}K_{0.6}$ catalyst, three diffraction peaks at 21.7, 27.8, and 39.0 were observed, which might be related to the structure of rhombohedral K–Mo–S in addition to K_2CO_3. Generally, K_2CO_3 would transform into K–Mo–S phase, which was related to catalytically active sites for alcohol synthesis. There were also some weak diffraction peaks at 2θ (degree) = 31.4, 37.3, 47.3, and 54.8, which were related to the second phase of CoS_x such as Co_9S_8 [28]. However, the addition of La, Y, or Ce caused strong diffraction peak intensities at 2θ values of 27.8 and 39.0 with the apparent decrease of the diffraction peak intensities of CoS_x phase. And the K–Mo–S peak intensities also became stronger with the increase of La/Mo molar ratio. On the other hand, due to the low La content, no diffraction peak related to the La-contained phases was observed. All these results suggested that the addition of La effectively inhibited the formation of separated cobalt sulfides and simultaneously enhanced the formation of K–Mo–S phases.

Table 1 Results of BET and EDS measured the metal composition on the catalyst surface and surface area of the prepared catalysts

Cat.	BET/m^2/g	Elements (atom%)					Analysis results (atomic ratio)			
		Mo	Co	La	K	S	S/Mo	Co/Mo	K/Mo	La/Mo
MoS_2	9.80	32.95	–	–	–	63.89	1.94	–	–	–
$MoCo_{0.5}K_{0.6}$	7.40	10.88	17.17	–	30.84	40.78	3.74	1.57	2.83	–
$La_{0.1}MoCo_{0.5}K_{0.6}$	7.64	23.13	10.59	2.21	15.36	45.20	1.95	0.46	0.66	0.096
$La_{0.2}MoCo_{0.5}K_{0.6}$	8.01	20.97	13.72	4.28	14.72	46.31	2.21	0.65	0.71	0.205
$La_{0.3}MoCo_{0.5}K_{0.6}$	3.62	21.06	11.83	5.86	13.13	48.12	2.28	0.56	0.63	0.278

3.3 Characterization of SEM and TEM

Figure 2 shows the SEM images of MoS_2, as-prepared catalyst $MoCo_{0.5}K_{0.6}$ and $La_{0.2}MoCo_{0.5}K_{0.6}$. Some remarkable differences were observed. For catalyst $MoCo_{0.5}K_{0.6}$ (Fig. 2b), the size and morphology of spongy particles were non-uniform, and the needle-like crystal particles were observed. For the $La_{0.2}MoCo_{0.5}K_{0.6}$ catalyst, however, no obvious needle-like particles was observed (Fig. 2c), which had uniform spongy particles size and morphology. The evident morphological differences between two catalysts suggested that La addition effectively enhanced the homogeneity and dispersion of modified MoS_2 based catalyst.

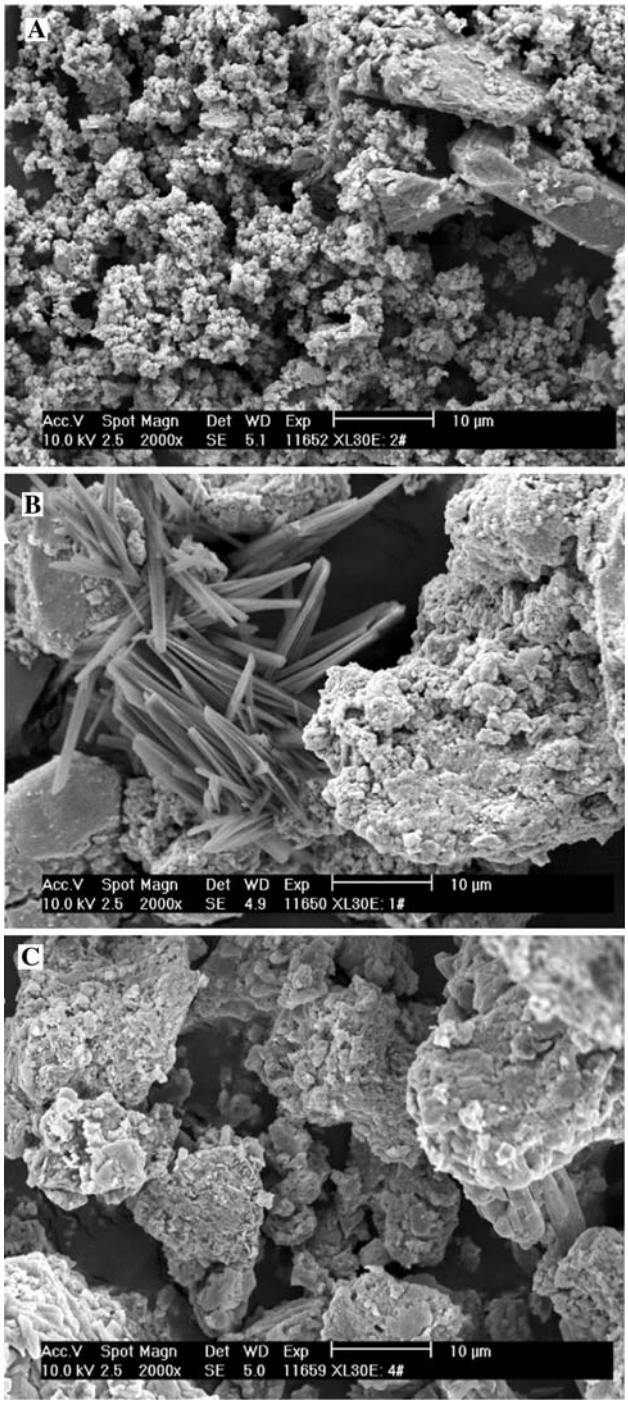

Fig. 2 The SEM images of MoS_2 and the unsupported Mo–Co–K sulfide catalyst. **a** MoS_2; **b** $MoCo_{0.5}K_{0.6}$; **c** $La_{0.2}MoCo_{0.5}K_{0.6}$

Figure 3 shows representative HRTEM micrographs of MoS_2, as-prepared $MoCo_{0.5}K_{0.6}$ and $La_{0.2}MoCo_{0.5}K_{0.6}$ catalyst. Table 2 shows the structural parameters of MoS_2 crystallites obtained by measuring the length and number of MoS_2 layers in each HRTEM photograph. The MoS_2 is characteristic random layers structure. The fringes observed in the photograph had a spacing of about 0.6 nm that was characteristic of the (002) basal planes of crystalline MoS_2 [29]. Each crystalline MoS_2 consists of average seven layers slabs with over 10 nm in length. For the $MoCo_{0.5}K_{0.6}$ catalyst, it only had stacked MoS_2 with average 3.4 layers thickness and around 6.1 nm length (Fig. 3b). However, for the $La_{0.2}MoCo_{0.5}K_{0.6}$ catalyst, the number of layers of the MoS_2 crystallites was about 5.3 with an average length 8.9 nm. This difference in structure clearly indicates that the $La_{0.2}MoCo_{0.5}K_{0.6}$ catalyst had much longer and more stacked MoS_2 crystallites than that in the $MoCo_{0.5}K_{0.6}$ catalyst.

3.4 Characterization of Raman

To further investigate the effect of La addition on the structure of the unsupported Mo–Co–K sulfide catalysts, the Laser Raman spectroscopy was performed; and its spectra are shown in Fig. 4. Three well-resolved bands at about 380, 400 and 449 cm^{-1}, respectively, were observed for all samples. According to literature [30], the bands at about 380 and 400 cm^{-1} are assigned to the characteristic of Mo–S stretching vibration in MoS_2; and the 449 cm^{-1} is assigned to the μ-S bridge vibration in MoS_2. Two new bands at 620 and 980 cm^{-1} appeared in the $MoCo_{0.5}K_{0.6}$ catalyst, which are attributed to the vibration of Co–S in CoS_x phases and Mo–S in Mo–Co–S phases [31], indicating that the separated cobalt sulfide phases existed on the $MoCo_{0.5}K_{0.6}$ catalyst. This observation was also in agreement with the XRD, EDS, and SEM characterization results. However, some obvious differences were observed in the $La_xMoCo_{0.5}K_{0.6}$ ($x = 0.1$, 0.2, and 0.3) catalyst. First, the intensity of peak at 620 cm^{-1}, assignable to the vibration of Co–S in CoS_x phases, decreased dramatically and the peak even disappeared with increasing the La/Mo molar ratio. Second, the peak at 980 cm^{-1}, assignable to the vibration of Mo–S in Mo–Co–S phases, shifted to 886, 899 and 930 cm^{-1}, respectively, with the increase of La/Mo molar ratio. Third, the band of ν (as) Mo–S in MoS_2 at 310 cm^{-1} appeared and its intensity increased with the

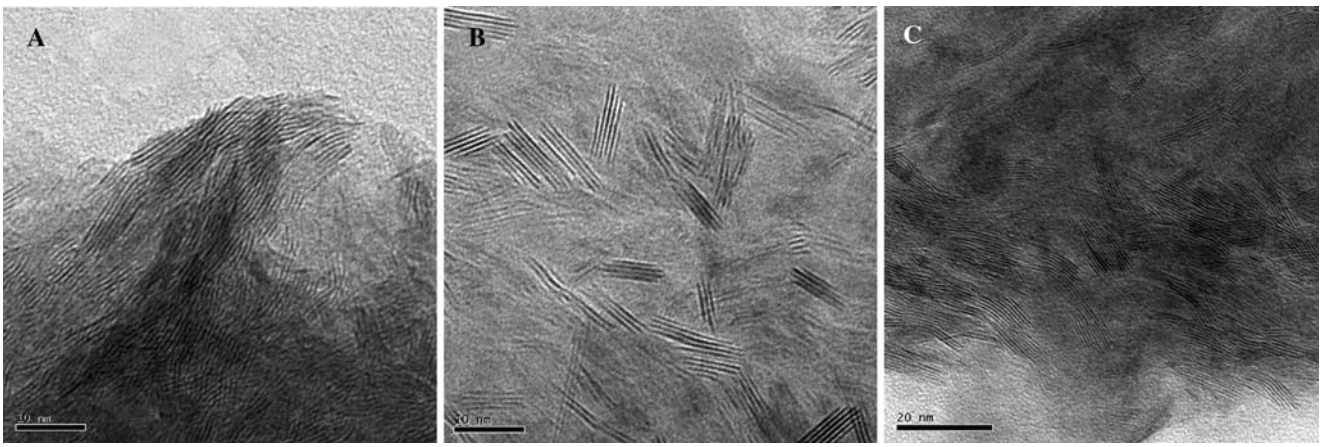

Fig. 3 The high-resolution TEM images of MoS_2 and the unsupported Mo–Co–K sulfide catalyst. **a** MoS_2; **b** $MoCo_{0.5}K_{0.6}$; **c** $La_{0.2}MoCo_{0.5}K_{0.6}$

Table 2 CO conversion and selectivity to alcohols with various catalysts

Cat.	CO conversion/C%	Alcohol STY/g/mL/h	Selectivity/C%			Alcohol distribution/C%			
			$C_{2+}OH$	Hc	ROH	MeOH	EtOH	PrOH	BuOH
$MoCo_0K_{0.6}$	7.8	0.033	23.9	43.4	56.6	52.1	37.2	10.1	0.6
$MoCo_{0.1}K_{0.6}$	13.6	0.072	42.6	28.9	71.1	40.1	46.0	13.8	0.1
$Ce_{0.2}MoCo_{0.1}K_{0.6}$	18.6	0.102	41.8	26.7	73.3	39.7	52.2	7.8	0.3
$Y_{0.2}MoCo_{0.1}K_{0.6}$	16.5	0.085	42.9	30.7	69.3	35.3	55.2	8.9	0.4
$La_{0.1}MoCo_{0.1}K_{0.6}$	6.9	0.094	41.8	26.8	73.2	39.7	50.2	8.6	1.5
$La_{0.2}MoCo_{0.1}K_{0.6}$	17.2	0.096	43.0	24.8	75.4	39.3	53.4	7.1	0.2
$La_{0.3}MoCo_{0.1}K_{0.6}$	15.9	0.091	39.4	24.7	75.3	43.3	46.5	9.0	1.1
$La_{0.6}MoCo_{0.1}K_{0.6}$	11.0	0.056	25.1	34.3	65.7	57.8	32.3	9.3	0.6

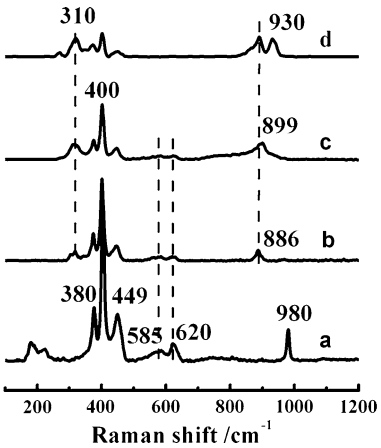

Fig. 4 The Raman spectra of the unsupported Mo–Co–K sulfide catalyst. (a) $MoCo_{0.5}K_{0.6}$; (b) $La_{0.1}MoCo_{0.5}K_{0.6}$; (c) $La_{0.2}MoCo_{0.5}K_{0.6}$; (d) $La_{0.3}MoCo_{0.5}K_{0.6}$

increase La/Mo molar ratio. The discrepancy of Raman vibration values might be the possibility that the La species affected the electron structure between Co and Mo and concentration of active sites of Mo–Co–S phases after addition of La into the $MoCo_{0.5}K_{0.6}$ catalyst.

3.5 Characterization of XPS

Figure 5 shows the Mo3d and Co2p-XPS spectra for MoS_2, $MoCo_{0.5}K_{0.6}$, and $La_{0.2}MoCo_{0.5}K_{0.6}$. In all cases, the binding energy for $Mo3d_{3/2}$ and $Mo3d_{5/2}$ were around 229.0 and 232.2 eV (B. E.), respectively, which could be assigned to MoS_2. A slight shift of $Mo3d_{3/2}$ binding energy toward lower value was observed for the $MoCo_{0.5}K_{0.6}$ catalyst, which was due to a strong electron transfer from Co to Mo. Compared with the $MoCo_{0.5}K_{0.6}$ catalyst, the binding energy of $Mo3d_{5/2}$ further shifted toward lower value and the peak area increased in the $La_{0.2}MoCo_{0.5}K_{0.6}$ catalyst, indicating that La enhanced the interaction between Co and Mo and the Mo^{4+} concentration on the surface of catalyst. No significant difference was observed in the binding energy of Co2p between $MoCo_{0.5}K_{0.6}$ and $La_{0.2}MoCo_{0.5}K_{0.6}$. The Co ($2p_{3/2}$, $2p_{1/2}$)-XPS peaks appeared at around 780.6 and 796.8 eV with their area ratio being approximately 2. These values are characteristics of the Co sulfide species interacting with Mo species to form Mo–Co–S composite species [32]. And the $La_{0.2}MoCo_{0.5}K_{0.6}$ catalyst showed a higher $Co2p_{3/2}$ peak area than that in the $MoCo_{0.5}K_{0.6}$ catalyst.

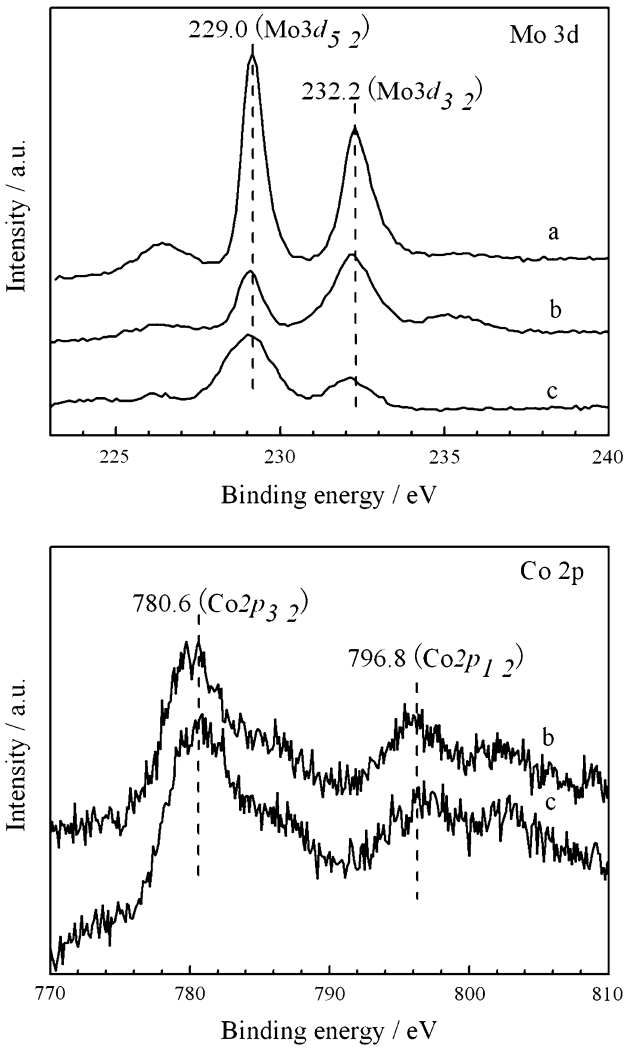

Fig. 5 The XPS spectra of MoS_2 and catalysts for different elements. (a) MoS_2; (b) $MoCo_{0.5}K_{0.6}$; (c) $La_{0.2}MoCo_{0.5}K_{0.6}$

3.6 Catalytic Activity

3.6.1 Effect of the Rare Earth

The CO conversion and selectivity to ethanol over the various catalysts are listed in Table 3. The $MoCo_{0.5}K_{0.6}$ catalyst exhibited a much lower CO conversion and selectivity to ethanol. However, the Mo–Co–K sulfide catalysts promoted by La, Y, or Ce showed much higher both CO conversion and selectivity to ethanol under identical reaction conditions. For instance, the CO conversion was increased from 13.6% to 17.2, 16.5 and 18.6%, and the selectivity to ethanol was enhanced form 46.0% to 53.4, 55.2 and 52.2%, after the addition of La, Y and Ce, respectively, in the case of M/Mo molar ratio at 0.2. The results indicate that the addition of rare earth exerted an important role in increasing both CO conversion and selectivity to ethanol. As mentioned above, much more catalytically active species formed on the surface of catalysts after the addition of La, and as a result, it enhanced effectively the catalytic activity.

Table 3 MoS_2 structural parameters of the different catalysts

Catalyst	L_{av}^{a} (nm)	N_{av}^{b}	N_{av}/L_{av} (nm^{-1})
MoS_2	10.2	7.0	0.69
$MoCo_{0.5}K_{0.6}$	6.1	3.4	0.56
$La_{0.2}MoCo_{0.5}K_{0.6}$	8.9	5.3	0.60

[a] L_{av}: average length of an MoS_2 stack

[b] L_{av}: average number of MoS_2 layers per stack

On the other hand, CO conversion and selectivity to ethanol were also influenced by the changes of La/Mo molar ratio (listed in Table 3). Both of CO conversion and selectivity to ethanol increased with increasing the molar ratio of La/Mo, whereas too high a molar ratio of La/Mo lowered the CO conversion and selectivity to ethanol. The highest catalytic activity was obtained with the La/Mo molar ratio at 0.2.

3.6.2 Effect of the Reaction Temperature

Figure 6 shows the effect of the reaction temperature on CO conversion and selectivity over the $La_{0.2}MoCo_{0.5}K_{0.6}$ and $MoCo_{0.5}K_{0.6}$ catalyst. Similar reaction-chemical behavior was observed on both catalysts. An increased CO conversion was observed with increasing the reaction temperatures for both $MoCo_{0.5}K_{0.6}$ and $La_{0.2}MoCo_{0.5}K_{0.6}$ catalysts. The selectivity to total alcohols decreased sharply for both catalysts with the reaction temperature raised from 300 °C to 340 °C. Compared with the $MoCo_{0.5}K_{0.6}$ catalyst, the $La_{0.2}MoCo_{0.5}K_{0.6}$ catalyst exhibited a higher CO conversion and selectivity to total alcohols under identical reaction conditions. Figure 6b shows the selectivity to alcoholic products over the $MoCo_{0.5}K_{0.6}$ and $La_{0.2}MoCo_{0.5}K_{0.6}$ catalysts. The major alcoholic products consisted of MeOH, EtOH, and PrOH in our system. With the increase of reaction temperature, the selectivity to MeOH decreased magnificently along with increasing EtOH and PrOH selectivity for both catalysts, whereas the selectivity to EtOH approached a miximun value at 330 °C. As shown in Fig. 6b, the selectivity to EtOH on the $La_{0.2}MoCo_{0.5}K_{0.6}$ catalyst was higher than that on the $MoCo_{0.5}K_{0.6}$ catalyst during the whole process.

3.6.3 Effect of the Reaction Velocity

The effect of velocity (GHSV) of reactants on CO conversion and selectivity was also investigated in the range from 1,000 to 3,750 h^{-1}. The results are presented in Fig. 7. Compared with the $MoCo_{0.5}K_{0.6}$ catalyst, a higher

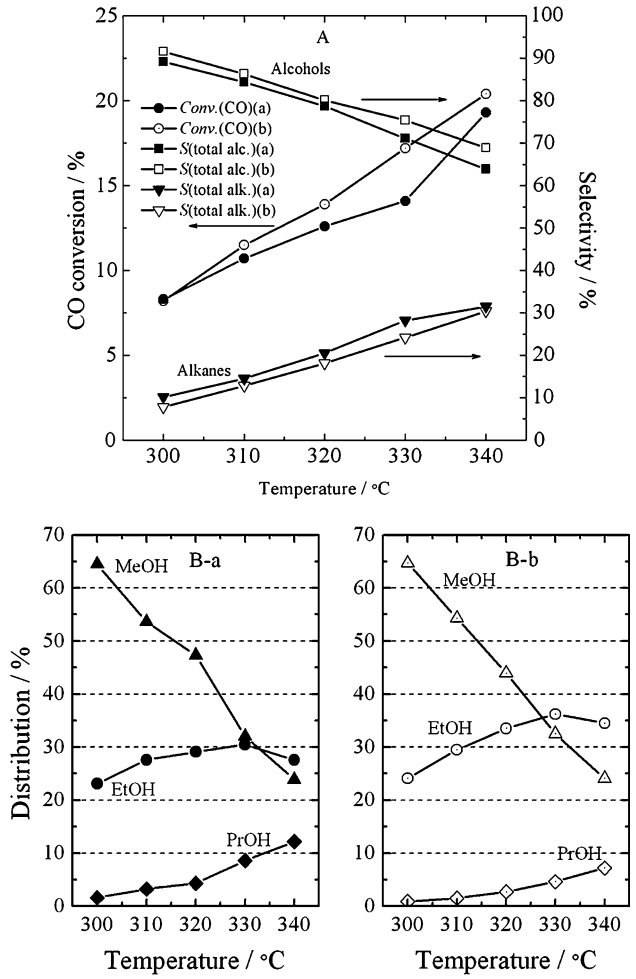

Fig. 6 Effect of reaction temperature on CO conversion and selectivity over catalyst: **a** $MoCo_{0.5}K_{0.6}$; **b** $La_{0.2}MoCo_{0.5}K_{0.6}$

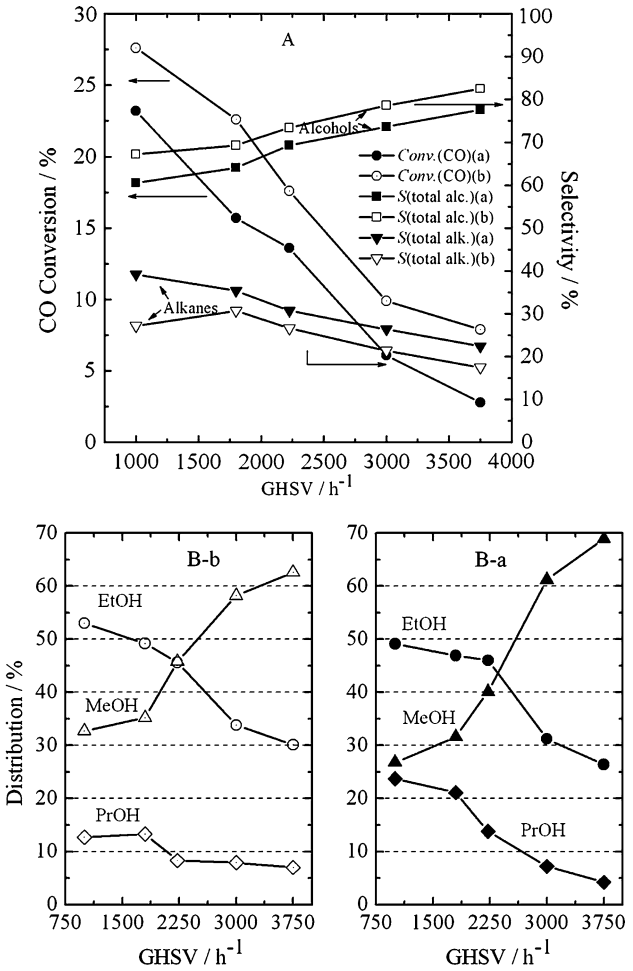

Fig. 7 Effect of reaction velocity on CO conversion, selectivity and product distribution over catalyst: **a** $MoCo_{0.5}K_{0.6}$; **b** $La_{0.2}MoCo_{0.5}K_{0.6}$

CO conversion and selectivity to alcohols could be obtained over the $La_{0.2}MoCo_{0.5}K_{0.6}$ catalyst during the whole process. With increasing space velocity, the contact time between reactant feed and active species on the catalyst surface decreased, resulting in the decrease of CO conversion. Due to the decreasing probability of the CO insertion and dissociation under a higher space velocity, the selectivity to C_{2+}-alcohols, i. e. EtOH and PrOH also decreased, and correspondingly, the selectivity to MeOH increased. But the selectivity to total alcohols kept increasing with the increase of the space velocity.

3.6.4 The Stability of Catalyst

The time-on-stream activity and selectivity of the $La_{0.2}MoCo_{0.5}K_{0.6}$ catalyst is reported in Fig. 8. No obvious deactivation was observed for CO conversion and selectivity to alcohols after the reaction for 27 days. The results

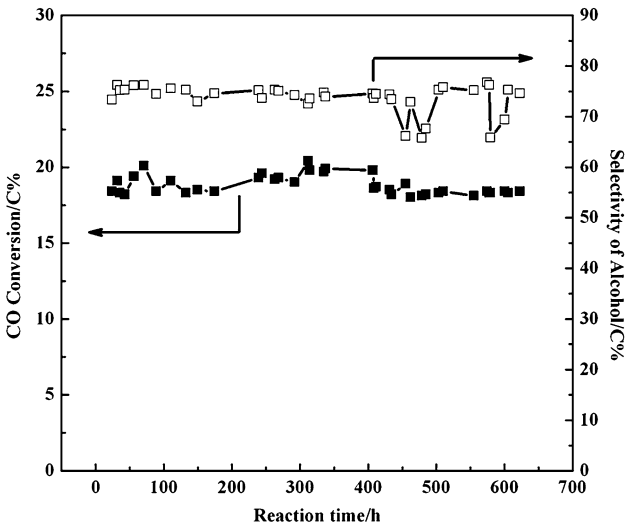

Fig. 8 The stability result of $La_{0.2}MoCo_{0.5}K_{0.6}$ catalyst

indicated that the $La_{0.2}MoCo_{0.5}K_{0.6}$ catalyst had strong stability for the synthesis of mixed alcohols from syngas.

4 Conclusion

Effects of lanthanum promotion on the surface properties and higher alcohols synthesis activity of the unsupported Mo–Co–K sulfide catalysts prepared through ultrasonic technology in non-aqueous medium were studied. La addition significantly affected the surface morphology and structure of catalysts, inhibited the formation of separated CoS_x crystal particles, and enhanced the dispersion of Co species and catalytically active sites concentration such as Mo–Co–S mixture phases on the catalyst surface. Compared with the $MoCo_{0.5}K_{0.6}$ catalyst, the $La_{0.2}MoCo_{0.5}K_{0.6}$ catalyst exhibited both higher CO conversion and selectivity to total alcohols under identical reaction conditions. And the $La_{0.2}MoCo_{0.5}K_{0.6}$ catalyst also showed strong stability for the synthesis of mixed alcohols from syngas.

Acknowledgments This work was supported by China Postdoctoral Science Foundation. The author thanks Dr. Tang Dingliang (Xiamen University, Fujian, P R China) for the XPS experiments.

References

1. Iranmahboob J, Hill DO, Toghiani H (2002) Appl Catal A 231(1–2):99
2. Fujimoto K, Oba T (1985) Appl Catal 13(2):289
3. Tatsumi T, Muramatsu A, Tominaga H (1987) Appl Catal 60(9):3157
4. Li DB, Yang C, Zhang HR, Li WH, Sun YH, Zhong B (2005) Top Catal 32(3–4):233
5. Li DB, Yang C, Zhang HR, Li WH, Sun YH, Zhong B (2004) Stud Surf Sci Catal 147:391
6. Li ZR, Fu YL, Bao J, Jiang M, Hu TD, Liu T, Xie YN (2001) Appl Catal A 220(1–2):21
7. Ma XM, Lin GD, Zhang HB (2006) Catal Lett 111:141
8. Wu XM, Guo YY, Zhou JM, Lin GD, Dong X, Zhang HB (2008) Appl Catal 340:87
9. Dong X, Zhang HB, Lin GD, Yuan YZ, Tsai KR (2003) Catal Lett 85(3–4):237
10. Zhang HB, Dong X, Lin GD, Liang XL, Li HY (2005) Chem Commun 5094
11. Li ZR, Fu YL, Jiang M, Hu TD, Liu T, Xie YN (2001) J Fuel Chem Technol 29:149
12. Li XG, Feng LJ, Liu ZY, Zhong B, Dadyburjor DB, Kugler EL (1998) Ind Eng Chem Res 37(10):3853
13. Li DB, Zhao N, Qi HJ, Li WH, Sun YH, Zhong B (2005) Catal Commun 6(10):674
14. Tien-Thao N, Zahedi-Niaki MH, Alamdari H, Kaliagine S (2007) J Catal 245:348
15. Tien-Thao N, Zahedi-Niaki MH, Alamdari H, Kaliagine S (2007) Appl Catal A 326:152
16. Xiang ML, Li DB, Qi HJ, Li WH, Zhong B, Sun YH (2007) Fuel 86:1298
17. Xiang ML, Li DB, Qi HJ, Li WH, Zhong B, Sun YH (2006) Fuel 85:2662
18. Smith KJ, Herman RG, Klier K (1990) Chem Eng Sci 45:2693
19. Li ZR, Fu YL, Jiang M (1999) Appl Catal 187:187
20. Woo HC, Kim YG (1993) Catal Lett 20:221
21. Li ZR, Fu YL, Jiang M, Xie Y, Hu T, Liu T (2000) Catal lett 65:43
22. Topsoe H, Clausen BS, Candia R, Wivel C, Morup S (1981) J Catal 68:433
23. Upton BH, Chen CC, Rodriguez NM, Baker RTK (1993) J Catal 141:171
24. Wang DZ, Cheng XP, Huang ZR, Wang XZ, Peng SY (1991) Appl Catal 77(1):109
25. Lansink Rotgerink HJG, Paalman RPAM, van Omen JG, Ross JRH (1988) Appl Catal 45(2):257
26. Li DB, Yang C, Qi HJ, Zhang HR, Li WH, Sun YH, Zhong B (2004) Catal Commun 5:605
27. Ogawa Y, Toba M, Yoshimura Y (2003) Appl Catal A 246:213
28. Park KT, Kong J (2002) Top Catal 18:175
29. Iwata Y, Sato K, Yoneda T, Miki Y, Sugimoto Y, Nishijiama A, Shimada H (1998) Catal Today 45:353
30. Woo HC, Nam IS, Lee JS, Chung JS, Lee KH, Kim YG (1992) J Catal 138:525
31. Bian GZ, Fu YL, Ma YS (1999) Catal Today 51:187
32. Okamoto Y, Ochiai K, Kawano M, Kobayashi K, Kubota T (2002) Appl Catal A 226:115